

# Haptic Interface With Force and Torque Feedback for Robot-Assisted Endovascular Catheterization

Xianqiang Bao , Member, IEEE, Shuxiang Guo , Fellow, IEEE, Cheng Yang, and Lingling Zheng 

**Abstract**—Robot-assisted endovascular catheterization is generally performed remotely; interventionists perceive the operation status and control surgical instruments through haptic interfaces. Our main objective is to create a haptic interface that retains interventionists' prior clinical operating experience, including motion perception, force feedback, torque feedback, tactile sensation, and operating mode. The haptic interface can capture the interventionists' operation of both catheters and guidewires and generate force and torque to assist the interventionists in performing surgeries on the master side. The tactile sensation and traditional operating mode are retained by adopting real commercial catheters/guidewires as the operating handles and designing a cooperative operation paradigm. A novel sensor-based force generation solution and a torque generation method with a pantograph mechanism were proposed to improve the force and torque feedback accuracy. Laboratory and animal experiments illustrated the good

feasibility of the proposed haptic interface. The proposed haptic interface has a good performance and can enable interventionists to utilize their prior accumulated clinical operating experience. This research could provide a reference for the design of haptic interfaces, and the developed haptic interface has the potential for use in robot-assisted endovascular catheterization.

**Index Terms**—Animal experiment, endovascular catheterization, force feedback, haptic interface, tactile sensation, torque feedback.

## I. INTRODUCTION

ENDOASCULAR catheterization has become increasingly necessary recently and has been widely used due to the reduced risk of injury and increased safety for patients [1]. However, interventionists are apt to suffer from strain injuries with repetitive procedures and long operations. In addition, they are at risk from radiation because endovascular catheterization is performed under X-rays guidance [2]. Therefore, robot-assisted endovascular catheterization is potentially useful and has received increasing attention [2]. During robot-assisted endovascular catheterization, interventionists and patients are separated: the interventionist operates the master interface on the master side (in another place outside the operating room) while the slave manipulator duplicates the interventionist's operations to perform surgery on the patient on the slave side (in the operating room) [3]. The master interface and slave manipulator are two vital components for robot-assisted endovascular catheterization, and much research has been devoted to them for decades.

Catheters and guidewires are both needed in endovascular catheterization (see Fig. 1), especially for some complex surgeries since catheters can provide support and assistance to guidewires, while guidewires will be used as guidance and positioning instruments [4]. Catheters and guidewires move forward or backward and rotate in blood vessels, and interventionists will sense force and torque caused by the linear movement and rotation of catheters and guidewires. So, in robot-assisted endovascular catheterization, the master interface needs to capture the linear movement and rotation of both catheters and guidewires, and generate force and torque feedback (discussed in Section II) [3]. In [5], a master interface was developed to control the robotic arm of the CorPath GRX robotic system. Wang et al. [6] proposed a master interface to

Manuscript received 14 December 2022; revised 15 April 2023; accepted 23 June 2023. Recommended by Technical Editor D. Oetomo and Senior Editor H. Qiao. This work was supported in part by the National High-tech Research and Development Program (863 Program) of China under Grant 2015AA043202 and in part by the National Key Research and Development Program of China under Grant 2017YFB1304401. (Corresponding authors: Shuxiang Guo; Lingling Zheng.)

This work involved human subjects or animals in its research. Approval of all ethical and experimental procedures and protocols was granted by the Shanghai Changhai Hospital Ethics Committee under Application No. CHEC20212-233 and the Institutional Review Board at Kagawa University under Application No. 01-011.

Xianqiang Bao is with the Key Laboratory of Convergence Medical Engineering System and Healthcare Technology, Ministry of Industry and Information Technology, Beijing Institute of Technology, Beijing 100081, China, and also with the Department of Biomedical Engineering, King's College London, WC2R 2LS London, U.K. (e-mail: xianqiang.bao@kcl.ac.uk).

Shuxiang Guo is with the Department of Electronic and Electrical Engineering, Southern University of Science and Technology, Shenzhen 518055, China, and also with the Key Laboratory of Convergence Medical Engineering System and Healthcare Technology, Ministry of Industry and Information Technology, Beijing Institute of Technology, Beijing 100081, China (e-mail: guo.shuxiang@sustech.edu.cn).

Cheng Yang is with the Key Laboratory of Convergence Medical Engineering System and Healthcare Technology, Ministry of Industry and Information Technology, Beijing Institute of Technology, Beijing 100081, China (e-mail: 3495367309@qq.com).

Lingling Zheng is with the School of Information Engineering and the School of Artificial Intelligence, Nanjing Xiaozhuang University, Nanjing 211171, China (e-mail: zhenglingling2018@outlook.com).

Color versions of one or more figures in this article are available at <https://doi.org/10.1109/TMECH.2023.3290492>.

Digital Object Identifier 10.1109/TMECH.2023.3290492

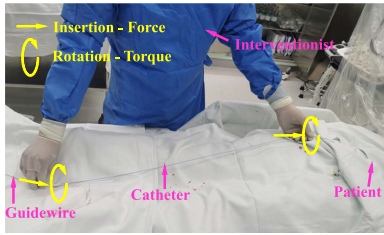


Fig. 1. Endovascular catheterization performed by interventionalists with one hand operating catheters and the other hand operating guidewires.

capture operations and dominate four manipulators. These two master interfaces all consist of several buttons and joysticks, which will fail to utilize the existing operating experience of interventionalists since this operating mode completely differs from the traditional operation in endovascular catheterization and the buttons or joysticks cannot provide tactile sensation (of real catheters and guidewires) to interventionalists. Similarly, Hooshiar et al. [7] developed a wearable device to capture rotations for robot-assisted interventional surgery but still failed to utilize the existing operating experience. Tavallaei et al. [8] tried to use a special handle and knob as the interactive components. The performance was tested *ex vivo* and *in vivo* for catheter navigation and ablation delivery. This type of master interface would bring a better operating experience than buttons or joysticks but have a great difference from the traditional operation and lose the tactile sensation. In [9], an actual catheter was integrated into the master interface and used as the operating handle. This catheter-based operating handle has the performance characteristics known to interventionalists and can retain the tactile sensation. Sankaran et al. [10] also developed a master interface by using the actual catheter. However, the tactile sensation was kept in [9] and [10] when using the real catheter, but the force sensation was still lost due to the lack of force or torque feedback.

To retain the force sensation, many researchers used commercial haptic devices as the master interface. For example, in [11] and [12], a commercial haptic device (Omega 3, 3D Systems, Inc., USA) was employed to capture interventionalists' operations and produce force feedback. Although it is able to provide high-precision force feedback, the two following shortcomings will limit its further applications. 1) This commercial haptic device is a universal interface whose operating mode significantly differs from the traditional operation in endovascular catheterization. 2) Most of the common commercial haptic devices, such as those used in [4], [11], [12] can only provide force feedback rather than both force and torque feedback. Meanwhile, some researchers abandoned commercial devices and tried to develop master interfaces with force feedback by themselves. In [13], a master interface was designed to manipulate the insertion and rotation of the catheter and the guidewire. It uses two dc motors to produce reflection force and make compensation for the dynamic inertial load. A master interface composed of a handle, a parallel mechanism, and two motors, was proposed in [14]. The handle mounted on the parallel mechanism transmitted the force generated by the motors to

the operator. Moreover, Cha et al. [15] also designed a master interface with 7 degrees of freedom by combining a double four-bar structure and a five-bar structure. Feng et al. [16] developed a console to control the slave manipulator. The console consists of several buttons and a handle. These buttons allow the slave manipulator to rotate the guidewire in the radial direction, and the handle captures linear displacement and produces force feedback. In [17], a magnetic powder brake was integrated into the master interface and used to generate force for operators. Operators can grasp a sleeve and move or rotate it. However, these master interfaces only restore part of the force sensation due to the lack of torque feedback and completely lose the tactile sensation because the operating handle differs from the real catheters and guidewires. In our previous research [18], [19], to achieve both tactile and force sensation for interventionalists, we investigated an MR fluids-based haptic interface using real catheters. This haptic interface has the ability to capture interventionalists' operations but only generates force feedback, which has a coupling relationship with torque feedback. Moreover, most of the existing master interfaces, for example, in [20], [21], [22], [23], and our previous research [24], are only developed for the catheter or guidewire operations and seem to be able to be used for both catheter and guidewire operations when two of them are employed simultaneously. In traditional surgical procedures, guidewires pass through and are located in catheters. Simultaneously using two such master interfaces will also result in a different operating mode from the traditional one.

In order to meet the requirements of various operations in endovascular catheterization, a master interface is required to capture both the catheter and guidewire operations. Also, tactile sensation, force sensation (including force and torque feedback), and traditional operating mode, need to be retained to improve the operation safety and utilize the prior accumulated clinical operating experience of interventionalists. The existing research, unfortunately, did not address all these limitations above, and only several of these limitations were overcome.

In this research, to overcome all the limitations mentioned above, we propose a novel haptic interface, which can capture the linear displacement and rotation of both catheters and guidewires, produce force and torque feedback, and retain the tactile sensation and traditional operating mode. The main contributions of this research can be summarized as follows.

- 1) We propose integrating the catheter and guidewire operations and force and torque feedback into a haptic interface, which can collect interventionalists' operating data on the master side and reflect operating information in the blood vessels more comprehensively (i.e., all the force sensation). More comprehensive operating information can exchange between the master side and slave side, and thus, the operability and safety will potentially be increased.
- 2) The proposed haptic interface simulates interventionalists' operation paradigm and uses actual catheters and guidewires as the operating handles. This highly simulated design retains the tactile sensation and traditional operating mode. It will enable interventionalists to utilize their prior accumulated clinical operation experience.

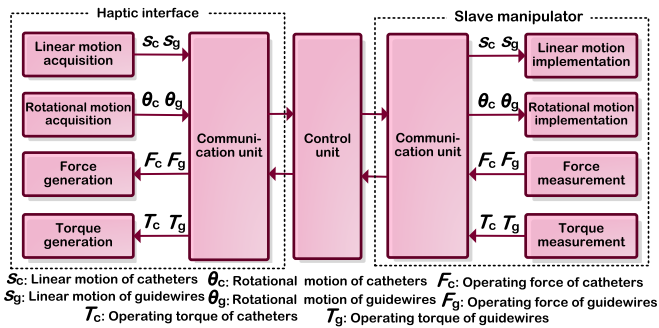


Fig. 2. Block diagram of robot-assisted endovascular catheterization systems.

- 3) A novel sensor-based force generation solution and a torque generation method with a pantograph mechanism are proposed to achieve force and torque feedback with the required accuracy for catheterization. These two methods allow interventionists to experience the surgical conditions more realistically, thereby potentially improving the safety and efficiency of operations.

The rest of this article is organized as follows. Clinical requirements are described in Section II. Section III presents the design details. Modelling and analysis are described in Section IV. Performance evaluation experiments are conducted in Section V, and animal experiments are detailed in Section VI. Finally, Section VII conclude this article.

## II. CLINICAL REQUIREMENTS

As shown in Fig. 1, interventionists operate the catheter with one hand and manipulate the guidewire with the other hand. Catheters and guidewires are manipulated by pull and push with the operating force and by rotation with the operating torque. To utilize the interventionists' prior accumulated clinical operation experience, the haptic interface should be configured in an operating mode consistent with traditional procedures (see Fig. 1). The operating mode requirement includes the following specific aspects.:

- 1) operation types (performing simultaneous operations of both catheters and guidewires with linear and rotational motions);
- 2) the arrangement of operating handles (concentric layout);
- 3) the available operating space (with a catheter length of up to 900 mm and an operating space set at 300 mm to minimize frequent retractions);
- 4) the tactile sensation of the operating handles (consistent with the perception of actual catheter and guidewire).

In this research, for ease of distinction, the tactile sensation is defined as the sense of touch to the object's surface, such as the perception of texture, shape, size, and flexibility of objects.

In the teleoperated robot-assisted endovascular catheterization system, as shown in Fig. 2, the haptic interface captures interventionists' operations, i.e., linear motion and rotational motion of catheters and guidewires ( $s_c$ ,  $s_g$ ,  $\theta_c$ , and  $\theta_g$ ) on the master side and send this operating data to the control unit. The signals sent from the control unit flow into the slave manipulator

(on the slave side) that performs the motions of catheters and guidewires. Meanwhile, the slave manipulator measures the operating forces and torques of catheters and guidewires ( $F_c$ ,  $F_g$ ,  $T_c$ , and  $T_g$ ) and the haptic interface generates forces and torques on the master side according to the measured values. Consequently, the haptic interface is required to fulfil these sensing and feedback capabilities. [25], [26] indicate that human's force resolution is 0.06 N, and the just noticeable difference (JND) for torque is 12.7% at the reference of 60 mN•m. The bandwidth for controlling forces has been estimated to be approximately 2 Hz for forearms, while the bandwidth for force control of fingers is determined to be less than 6 Hz [25]. The operating force and torque during endovascular catheterization procedures generally will not exceed 3.2 N and 10 mN•m [27], [28]. [33] point out that, in a master-slave system, a low bandwidth (5–10 Hz) could be used from the hand controller to the slave, and a higher bandwidth (20–320 Hz) could be used from the slave to the hand controller. In addition, we have carried out laboratory, animal and in-human experiments [4], [19], [29], and based on the data and discussions with interventionists, acceptable sensing and feedback requirements for the haptic interface are determined to the following:

- 1) be able to measure the linear and rotational motions with errors less than 0.5 mm and 1°, respectively, with a bandwidth of 320 Hz;
- 2) produce force feedback in a range of 3.4 N with a resolution of 0.06 N and a bandwidth of 5 Hz;
- 3) generate torque feedback in a range of 12 mN•m with a resolution of 0.07 mN•m and a bandwidth of 5 Hz.

## III. DESIGN

### A. Design Overview

The overview of the proposed haptic interface is shown in Fig. 3. The haptic interface consists of a linear platform, a catheter operation module, and a guidewire operation module. The linear platform equipped with motors drives the catheter operation module and guidewire operation module in the linear direction. An actual commercial catheter used as the master catheter is connected to the catheter operation module, and an actual commercial guidewire used as the master guidewire is mounted on the guidewire operation module. Operators can manipulate the master catheter and master guidewire with both hands at the same time. The linear platform measures the linear motions of the master catheter and guidewire, and generates force feedback; the catheter operation module and guidewire operation module capture the rotations of the master catheter and guidewire, and generate torque feedback.

In traditional surgical procedures (see Fig. 1), guidewires need to pass through and be located in catheters. Therefore interventionists operate catheters near the puncture site of arteries while manipulating guidewires close to the end of catheters. In Fig. 3, with the proposed haptic interface, interventionists manipulate the master catheter near the catheter operation module and operate the master guidewire at the end of the catheter; meanwhile, the operating forces and torques of the catheter and guidewire are generated and fed back to interventionists' hands.

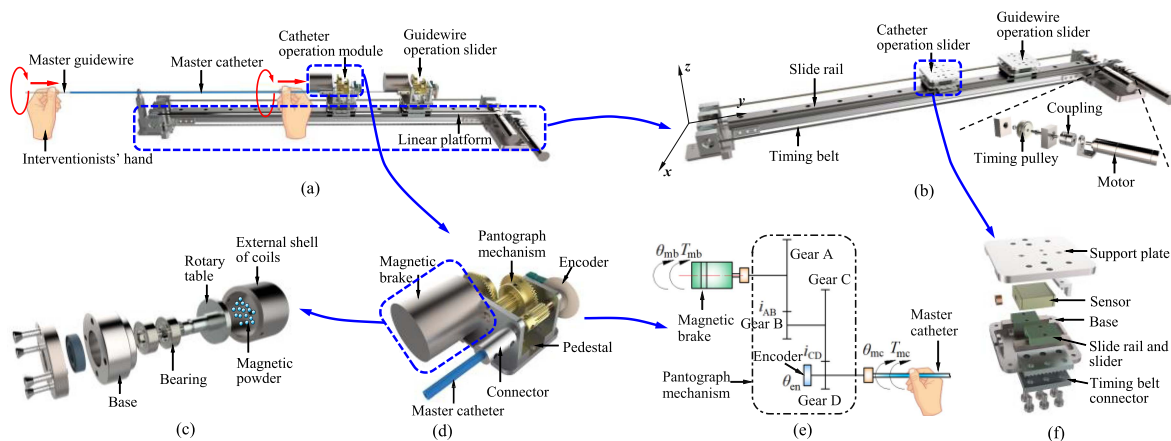


**Fig. 3.** Design details of the proposed haptic interface. (a) Overview. (b) Linear platform. (c) Exploded view of the magnetic brake. (d) Catheter operation module. (e) Kinematic diagram of the catheter operation module. (f) Exploded view of the catheter operation slider.

This operating mode is the same as that in traditional surgical procedures. This design paradigm, adopting real commercial catheters and guidewires and using the traditional operating mode, retains the tactile sensation and enables interventionists to utilize their prior accumulated clinical operation experience. Since the slave manipulator set in the operating room is remotely controlled by the haptic interface located in another place outside the operating room, it is unnecessary to implement a sterilization design for the haptic interface.

### B. Motion Acquisition

As shown in Fig. 3(b), the catheter operation slider/guidewire operation slider, on which the catheter operation module/guidewire operation module is mounted, moves forward or backward when interventionists pull or push the master catheter/guidewire. A timing belt (HTBN1290S2M-40, MISUMI, JP) meshing with a timing pulley (MTPBV32S2M040-A-P4, BEIDI, CN) is connected to the catheter operation slider/guidewire operation slider. The timing pulley links with a motor through a coupling (SCPS16-4-4, MISUMI, JP). An encoder (201937, Maxon, CHE) mounted on the motor captures the motion of the motor, and thus the linear motion of the catheter operation module/guidewire operation module can also be obtained. Since the master catheter/guidewire has the same linear motion as the catheter operation module/guidewire operation module, the interventionists' linear operation on the master side will be measured and sent to the control unit. Fig. 3(d) and (e) show the structure and kinematic diagram of the catheter operation module. The master catheter is connected to the shaft of gear D with a connector. An encoder (PF37, BOSHEN, CN) mounted on the pedestal is connected to the shaft of gear D and measures the rotation of the shaft, and thus, the rotation of the master catheter will be obtained. The guidewire operation module has the same working principle as the catheter operation module.

### C. Force Generation

Since dc servo motors can provide active control and simulate active force/motion output at a high update rate [30], in this

design, a motor solution was proposed to generate the force feedback. In Fig. 3(b), with the coupling, timing pulley, timing belt, and slider rail, the resistance produced by the motor can be transmitted to the catheter operation slider/guidewire operation slider. The master catheter/guidewire is set in the catheter operation module/guidewire operation module installed on the catheter operation slider/guidewire operation slider. So operators will experience force feedback in the y-direction when they grasp and manipulate the master catheter/guidewire. Frictions exist inevitably in these components (e.g., bearing, timing pulley, and slider rail), and thus the motor need to compensate for the external frictions. Considering the required compensation and the volume, weight, control accuracy, and capacity of the motor, we selected two motors (283831, Maxon, CHE) with gearboxes (416391, Maxon, CHE). Two motor drivers (ESCON 50/5, Maxon, CHE) were employed to drive them.

Owing to the operation characteristics of endovascular catheterization, this dc servo motor solution will have two disadvantages when used to produce force feedback applied to the master catheter/guidewire.

- 1) The master catheter/guidewire may move autonomously when not pushed or pulled by interventionists. Due to the catheters/guidewire bending in the blood vessels, the measured force value may not be zero when interventionists stop manipulating catheters/guidewires. The measured force will then be transmitted to drive the dc servo motors that propel the master catheter/guidewire through timing belts. The master catheter/guidewire might move autonomously when not employed by interventionists. These automatic movements are not friendly to interventionists and would be recognized as interventionists' operations and replicated by the slave manipulator, resulting in unsafe operations.
- 2) A lack of force closed-loop brings about limited force generation accuracy. DC servo motors mainly achieve closed-loop control through position closed-loop and velocity closed-loop. This indirect closed-loop control results in low accuracy of force generation. To address these two challenges discussed above, we propose a novel sensor-based solution that uses a force sensor to identify interventionists' intentions, measure the generated force, and use the measured force as the feedback variable. This solution is integrated with

the traditional force feedback using motors and is implemented by creating the catheter operation slider/guidewire operation slider.

Fig. 3(f) shows the internal structure of the catheter operation slider. The support plate set on the slider can move relative to the base with a slide rail. The support plate supports and fixes the catheter operation module. A force sensor (LSB200, FUTEK, US) driven by a sensor signal conditioner (AAA100, FUTEK, US) connects the support plate and the base. The base is connected to the timing belt by a timing belt connector. Since the generated force feedback is transmitted from the timing belt to the support plate, it can be measured directly by the force sensor and used for the closed-loop control variable. The operating force is produced by the interaction between interventionists and the master catheter/guidewire, and the measured force will be 0 if interventionists do not operate the master catheter/guidewire. The measured force value can be used to identify the interventionists' intentions and be adopted as a criterion to drive the motor. The criterion for motor control is expressed as follows:

$$u_{\text{mot}} = \begin{cases} 0, & |F_{\text{sens}}| \leq F_{\delta} \\ \Gamma(u_{\text{mot}}), & |F_{\text{sens}}| > F_{\delta} \end{cases} \quad (1)$$

where  $u_{\text{mot}}$  means the input control signal of the motor,  $F_{\text{sens}}$  is the force measured by the force sensor,  $F_{\delta}$  is the equivalent fluctuation value of force during operations, and  $\Gamma(u_{\text{mot}})$  represents the control signal generated based on the operating force measured on the slave side. Due to the instability of measurement and the randomness of external interference, the measured values will also fluctuate around 0 even though the signals are filtered. Therefore, instead of 0,  $F_{\delta}$  is regarded as the conditional criterion of (1).

#### D. Torque Generation

As shown in Fig. 3(d) and (e), the catheter operation module/guidewire operation module is developed to generate torque for the master catheter/guidewire. The catheter operation module consists of a magnetic brake, pantograph mechanism, pedestal, encoder, connector, and master catheter. The magnetic brake is developed and used to produce a resistive torque that is transmitted to the master catheter/guidewire through the pantograph mechanism and connector. As shown in Fig. 3(c), the magnetic brake comprises a base, bearing, rotary table, external shell of coils, and magnetic powder. Two bearings set in the base support the rotary table and enable it to rotate with almost no friction. The rotary table is located in the internal shell of coils which has magnetic powders and can generate resistive torque based on control signals. The resistive torque can be easily controlled by the current since it has an approximately proportional relationship with the current [31]. A gear train consisting of four gears (gears A–D) works as the pantograph mechanism that changes the output torque and rotation of the magnetic brake.

When magnetic brakes are used to provide resistive torques, they are commonly connected with the output mechanism or transmission mechanism directly. For example, Wang et al. [17] use a magnetic brake to generate force feedback through a

cable-driven mechanism. However, when the method is used to create forces/torques with small values, the frictions caused by the external environment affect or even submerge the output forces/torques because of the existence of slide rails or bearings in both the forces/torques generation and transmission mechanisms, and because of the demand to move significantly and frequently. Hence, the method presented in [17] will apply to the situation with relatively great forces/torques but has limitations in the force/torque feedback with small values. The method may not be suitable for generating force/torque feedback for endovascular catheterization since the operating torques are not that great (commonly less than 10 mN•m [27]). Besides, the torque generation accuracy in [17] is also affected by the magnetic hysteresis and initial resistive torque of magnetic brakes, and thus it may not meet the requirements in endovascular catheterization.

In this research, we employ the pantograph mechanism to improve the torque generation accuracy and reduce or eliminate the effect caused by friction. The pantograph mechanism can scale down the values of the frictions, initial resistive torque, and generated torque. The reduction of these frictions and torques will

- 1) lower the impact of the initial resistive torque of the magnetic brake;
- 2) reduce the effect of frictions;
- 3) enlarge the adjustment range of the input current, thereby improving the control accuracy of the output torque.

#### E. Platform Components and Prototype

In this research, real commercial catheters/guidewires are used as the master catheters/guidewires of the proposed haptic interface. Since various operations are required to be performed with catheters/guidewires of different sizes, the master catheters/guidewires are designed as replaceable ones to enable interventionists to utilize their accumulated clinical operation experience. The master catheters/guidewires can be replaced with the same types of catheters/guidewires used in the surgeries to be performed, and the connectors of different sizes will be replaced accordingly [see Fig. 3(d)]. The position where interventionists hold the master guidewire is not close to the guidewire operation slider. When micro guidewires are used as master guidewires, the force/torque applied to the master guidewire will differ from the generated one (desired value) due to the small stiffness of micro guidewires. Steel wires with high stiffness can be used to replace micro guidewires to eliminate this difference. Since guidewires are directly operated through torque devices (shown in Fig. 4) and the operating methods of torque devices grasping micro guidewires and steel wires are similar, this alternative solution would be acceptable for interventionists.

Fig. 5 shows the prototype of the proposed haptic interface. Most parts, including the linear platform, catheter/guidewire operation slider, and catheter/guidewire operation module, were fabricated from aluminum alloy, and the prototype was assembled and debugged in the laboratory. The proposed haptic interface has dimensions of 607 mm × 174 mm × 85 mm.

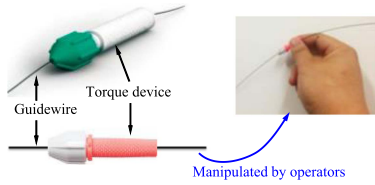


Fig. 4. Two types of torque devices grasping guidewires and the method that operators manipulating guidewires.

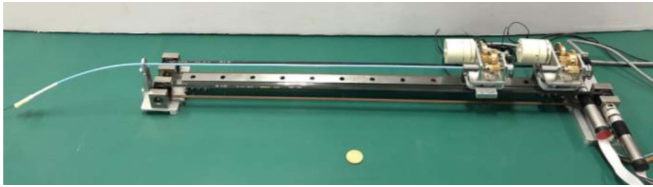


Fig. 5. Prototype of the proposed haptic interface.

#### IV. MODELING AND ANALYSIS

##### A. Linear Motion and Force

The linear motion of the master catheter/guidewire is measured by an encoder mounted on the motor. As shown in Fig. 3(b), the catheter operation module/guidewire operation module connected to the motor through the timing belt and timing pulley, has the same displacement as the master catheter/guidewire, and thus, the relation can be written as follows:

$$s_{mc} = \theta_t r_t \quad (2)$$

where  $s_{mc}$  means the displacement of the master catheter/guidewire,  $\theta_t$  is the rotation angle of the timing pulley, and  $r_t$  represents the radius of the timing pulley. Since the timing pulley is connected to a gearbox mounted on the motor through a coupling, the rotation angle of the timing pulley is expressed as follows:

$$\theta_t = \frac{\theta_m}{i_t} \quad (3)$$

where  $\theta_m$  is the rotation angle of the motor and  $i_t$  means the reduction ratio of the gearbox. The relationship between the displacement of the master catheter/guidewire and the reading of the encoder can be obtained by substituting (3) into (2)

$$s_{mc} = \frac{\theta_m r_t}{i_t}. \quad (4)$$

During the operation, the displacement of the master catheter/guidewire differs from the expected one applied by interventionalists due to the deformation of the master catheter/guidewire. As shown in Fig. 6(a), axial compression ( $\delta_1$ ) and vertical deflection ( $d_v$ ) are produced when the axial force ( $F_{ha}$ ) and vertical force ( $F_{hv}$ ) are applied by interventionalists' hands. Since the master catheter/guidewire is operated at low speed, we ignore the acceleration of the master

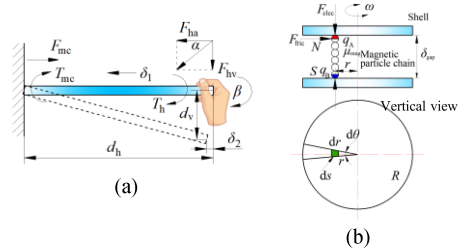


Fig. 6. Diagram of force analysis for (a) linear motion acquisition and (b) torque generation.

catheter/guidewire. The mechanical force relation can be expressed as follows:

$$\begin{bmatrix} F_{ha} \\ F_{hv} \end{bmatrix} = \begin{bmatrix} F_{mc} \\ F_{mc} \tan \alpha \end{bmatrix} \quad (5)$$

where  $F_{mc}$  is the force generated by the haptic interface and applied to the master catheter/guidewire and  $\alpha$  means the angle between  $F_{ha}$  and the resultant force. Based on the elastic deformation properties of rods, there are

$$\delta_1 = \frac{F_{ha} d_h}{E_{mc} S_{mc}} \quad (6)$$

$$d_v = \frac{F_{hv} d_h^3}{3 E_{mc} I_{mc}} \quad (7)$$

where  $d_h$  means the distance from interventionalists' hands to the end of the master catheter/guidewire,  $E_{mc}$  is Young's modulus of the master catheter/guidewire,  $S_{mc}$  is the cross-sectional area of the master catheter/guidewire, and  $I_{mc}$  means the moment of inertia of the master catheter/guidewire. According to the geometric relationship, the change caused by the vertical deflection to the axial displacement ( $\delta_2$ ) can be obtained by

$$\delta_2 = d_h - \sqrt{d_h^2 - d_v^2}. \quad (8)$$

The overall changes in the axial displacement ( $\delta_a$ ) is

$$\delta_a = \delta_1 + \delta_2. \quad (9)$$

The expected displacement applied by interventionalists ( $s_{ei}$ ) can be expressed as follows:

$$s_{ei} = s_{mc} - \delta_a. \quad (10)$$

Substituting (4)–(9) into (10) results in

$$s_{ei} = \frac{\theta_m r_t}{i_t} - \frac{F_{mc} d_h}{E_{mc} S_{mc}} - d_h \left( 1 - \frac{1}{E_{mc} I_{mc}} \sqrt{9 E_{mc}^2 I_{mc}^2 - F_{mc}^2 \tan^2 \alpha d_h^4} \right). \quad (11)$$

Since the force is generated by the motor and then transmitted to the master catheter/guidewire through the timing belt and slider, etc., frictions exist inevitably in these components and the relation can be written as follows:

$$F_{mc} = F_g - F_b - F_t - F_s \quad (12)$$

Where  $F_g$  is the force produced by the motor,  $F_b$  indicates the friction in bearings,  $F_t$  is the friction in the timing belt, and  $F_s$  represents the friction in the slider rail.  $F_g$  is generated when the motor produces torque and transmits it through the timing pulley, and the relationship can be written as follows:

$$F_g = \frac{T_m}{R_t} \quad (13)$$

where  $T_m$  means the torque produced by the motor and  $R_t$  is the equivalent radius of the timing pulley. We obtain  $T_m$  by a proportional-integral-derivative control as follows:

$$T_m = R_t K_1 (F_{des} - F_{meas} - F_f) + R_t K_2 \int (F_{des} - F_{meas} - F_f) dt + R_t K_3 d(F_{des} - F_{meas} - F_f) / dt + R_t F_{des} \quad (14)$$

where  $K_i$ ,  $i = 1, 2, 3$ , represents the feedback gain,  $F_{des}$  is the desired force,  $F_{meas}$  means the force measured by the sensor in the catheter/guidewire operation module, and  $F_f$  indicates the cumulative frictions encountered during force transmission, which can be expressed as  $F_f = F_b + F_t + F_s$ . These frictions can be ascertained through experimental means, as detailed in Section V-B.

### B. Rotational Motion and Torque

Fig. 3(e) shows the schematic diagram of rotational motion acquisition and torque generation. The rotary encoder is connected to the shaft of gear D jointed to the master catheter/guidewire by coupling and connector, and they have the same rotational motion. Thus, the rotation angle of the master catheter/guidewire ( $\theta_{mc}$ ) can be obtained by

$$\theta_{mc} = \theta_{en} \quad (15)$$

where  $\theta_{en}$  is the rotation angle of the encoder. Gear B meshing with gear A is installed on the same shaft as gear C that meshes with gear D. According to the meshing transmission characteristics, the rotation and torque relationships between gears are written as follows:

$$\begin{bmatrix} T_{mc} \\ \theta_{mc} \end{bmatrix} = \begin{bmatrix} i_{AB} i_{CD} T_{mb} \\ \theta_{mb} / (i_{AB} i_{CD}) \end{bmatrix} \quad (16)$$

where  $T_{mc}$  represents the torque applied to the master catheter/guidewire,  $i_{AB}$  means the reduction rate of gears A and B,  $i_{CD}$  represents the reduction rate of gears C and D,  $T_{mb}$  is the output torque of the magnetic brake,  $\theta_{mc}$  means the rotation angle of the master catheter/guidewire, and  $\theta_{mb}$  is the rotation angle of the magnetic brake.

Fig. 6(b) illustrates the operational principle of the magnetic brake. Magnetic particles form chains under the influence of an applied magnetic field, which can be analogized as chains possessing north (N) and south (S) poles at the extremities and no polarity in the central region. This chain can be considered as a pair of magnetic poles, and the electromagnetic force between these poles is given by the following:

$$F_{elec} = \frac{q_{mag}^2}{4\pi \times 10^{-6} \mu_{mag} \delta_{gap}^2} \quad (17)$$

where  $q_{mag}$  is the charge of the two magnetic poles which have equal charges  $q_A = q_B$ ,  $\mu_{mag}$  means the magneto-conductivity of magnetic particles, and  $\delta_{gap}$  represents the distance between the two magnetic poles. The shear force of magnetic particles can be interpreted as the friction occurring between the particles. The magnetization of magnetic particles intensifies as the magnetic field increases, leading to a larger electromagnetic force between the magnetic poles. According to Coulomb's friction law, the shear force of an individual magnetic particle chain is as follows:

$$F_{fric} = f_{mag} F_{elec} \quad (18)$$

where  $f_{mag}$  means the friction coefficient between magnetic particles. Assuming the number of magnetic particles per unit area is  $\xi_{mag}$ , the shear force generated by the magnetic powder per unit area is

$$\tau_{mag} = \xi_{mag} F_{fric}. \quad (19)$$

Substituting (17) and (18) into (19) results in

$$\tau_{mag} = \frac{f_{mag} \xi_{mag} q_{mag}^2}{4\pi \times 10^{-6} \mu_{mag} \delta_{gap}^2}. \quad (20)$$

Assuming the magnetic field intensity is  $B_{mag}$ , which serves as the effective external force inducing the formation of polarity in the magnetic particle, the magnetic field intensity per unit area can be equated to the total magnetic pole intensity formed by the magnetic particles in the unit area. Thus, we have

$$\xi_{mag} q_{mag} = \alpha B_{mag} \quad (21)$$

where  $\alpha$  is the conversion coefficient of the magnetic field. The torque generated by magnetic particles per unit area is

$$d T_{mag} = \tau_{mag} r ds \quad (22)$$

where  $T_{mag}$  is the torque generated by the magnetic particle,  $r$  is the distance between the magnetic particle chain and the center of rotation, and  $s$  is the area occupied by the magnetic particle. Substituting (20) and (21) into (22), we arrive at

$$T_{mag} = \iint \frac{\alpha^2 f_{mag} r^2 B_{mag}^2}{4\pi \times 10^{-6} \mu_{mag} \delta_{gap}^2 \xi_{mag}} dr d\theta. \quad (23)$$

Applying this equation to a cylindrical cavity with radius  $R$  and  $N$  rotary tables, the output torque of the magnetic brake is

$$T_{mb} = \frac{N \alpha^2 f_{mag} R^3}{6 \times 10^{-6} \mu_{mag} \delta_{gap}^2 \xi_{mag}} B_{mag}^2. \quad (24)$$

According to (24), the output torque is directly proportional to the square of the magnetic field. Since the magnetic field can be controlled via the current, it is possible to achieve precise control over the output torque of the magnetic brake by adjusting the current.

When the magnetic brake starts to work, the initial resistive torque of the magnetic brake is inevitably affected by the initial viscous resistance of the magnetic powder, bearing frictions, and assembly errors. Based on (16), the effect of the initial resistive torque of the magnetic brake on torque feedback ( $T_{eirt}$ ) is

$$T_{eirt} = i_{AB} i_{CD} T_{irt} \quad (25)$$

where  $T_{irt}$  is the initial resistive torque of the magnetic brake. Also, frictions from external components (except the magnetic brake) affect force feedback and they can be expressed as follows:

$$T_{ef} = i_{AB} i_{CD} T_{ff} + i_{CD} T_{fs} + T_{fmc} \quad (26)$$

where  $T_{ef}$  indicates the effect of the frictions on torque feedback,  $T_{ff}$  is the friction torque existing in the components between the first-stage gears and magnetic brake,  $T_{fs}$  is the friction torque existing in the components between the second-stage gears and first-stage gears, and  $T_{fmc}$  means the friction torque existing in the components between the master catheter/guidewire and second-stage gears. In this research,  $i_{AB}$  and  $i_{CD}$  are set to less than 1, so the effect of the initial resistive torque and all the other frictions on torque feedback will be scaled down. Considering the initial resistive torque and all the frictions, the actual torque applied to the master catheter/guidewire ( $T_{amc}$ ) is

$$T_{amc} = T_{mc} - T_{eirt} - T_{ef}. \quad (27)$$

Substituting (16) and (25)—(26) into (27) results in

$$T_{amc} = i_{AB} i_{CD} T_{mb} - i_{AB} i_{CD} T_{irt} - i_{AB} i_{CD} T_{ff} - i_{CD} T_{fs} - T_{fmc}. \quad (28)$$

Due to the torsional deformation of the master catheter/guidewire under torques, the rotation angles measured by the encoder differ from the expected rotation angles. To obtain the torsional deformation, we ignore the acceleration of the master catheter/guidewire that has low rotational speed during operations, and thus the relation can be written as follows:

$$\theta_{ei} = \theta_{en} + \frac{T_{amc} d_h}{G_{mc} I_{tmc}} \quad (29)$$

where  $\theta_{ei}$  is the expected rotation angles applied by interventionalists,  $G_{mc}$  indicates the shear modulus of the master catheter/guidewire, and  $I_{tmc}$  means the torsion constant of the master catheter/guidewire.

## V. PERFORMANCE EVALUATION

### A. Motion Acquisition

1) *Experimental Set-Up*: To test whether the proposed haptic interface can acquire the operating data accurately, experiments were carried out to evaluate the linear and rotational motion data collection performance. In the linear motion acquisition experiments, a linear stage with dc motors was used to generate linear motion [see Fig. 7(a)]. A connector was used to connect the slider and the catheter operation module. The catheter operation module was advanced 5 mm and stopped to measure the position data. Then the catheter operation module was retracted to the original position and repeated this movement ten times. The advance distances for each experiment were set as 5, 10, 15, 20, 30, 50, 70, and 100 mm, and the measurement data was recorded accordingly. The experimental set-up for rotational motion acquisition is shown in Fig. 7(b). The output shaft of the catheter operation module was connected to a dc motor through a coupling, and thus catheter operation module can be driven to target positions with the dc motor. The rotation

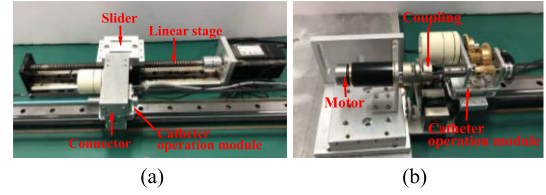


Fig. 7. Experimental set-up for evaluating (a) linear and (b) rotational motion acquisition.

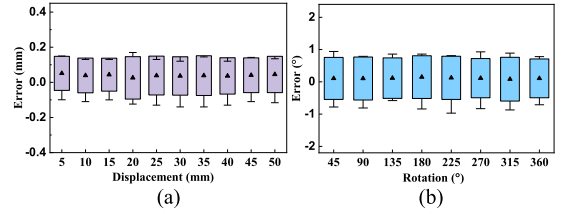


Fig. 8. Statistical data of (a) linear and (b) rotational motion acquisition.

angle of the output shaft was measured by the catheter operation module, and this rotation was repeated ten times. The desired positions were  $45^\circ$  with  $45^\circ$ -increments over a  $360^\circ$  range. Similar experiments were carried out to test the performance of the guidewire operation module.

2) *Results and Discussion*: Based on the experimental results, we found that the catheter operation module has the same performance as the guidewire operation module. This is mainly because the catheter operation module and guidewire operation module have the same structures and design parameters. To avoid repetition, we only selected the data of the catheter operation module for display (see Fig. 8). In the box plots, the whiskers indicate the maximum and minimum values; the two horizontal lines of the box represent standard deviations; the black triangles display the mean values. The linear accuracy and precision of the catheter operation module are 0.05 and 0.11 mm, respectively, and the rotational accuracy and precision of the catheter operation module are  $0.15^\circ$  and  $0.64^\circ$ , respectively. The performance evaluation of the catheter/guidewire operation modules demonstrated the ability of the proposed haptic interface to sense the interventionists' operation with the intended specifications, i.e., linear and rotational accuracy better than 0.5mm and  $1^\circ$ , respectively. In this research, we employed commercial encoders to directly measure the linear and rotational motions (see Section III-B). We obtained the operating frequencies of the encoders for linear and rotational motion measurements are 320 and 100 kHz, respectively. According to these results, the proposed haptic interface satisfies sensing and feedback requirement (1) proposed in Section II). The proposed haptic interface with the reported specifications can retain and utilize the dexterous skills possessed by the interventionists, and thus, the safety and efficiency of operation will be assured.

### B. Force and Torque Generation

1) *Experimental Set-Up*: To evaluate the accuracy of the force and torque generation, we investigated the performance by measuring the output forces and torques and comparing them

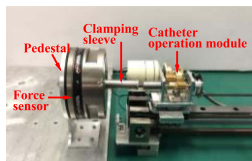


Fig. 9. Experimental set-up for force and torque generation experiments.

with the desired ones. A force sensor (Gamma, ATI Industrial Automation, Inc., USA) mounted on a pedestal was used to capture the generated forces and torques. As shown in Fig. 9, a clamping sleeve linked with the force sensor grasps a steel rod set in the connector of the catheter operation module. The expected forces and torques are shown in Fig. 10 with solid blue lines. To test the hysteretic characteristics of the torque generation, experiments were carried out by applying various input currents to the catheter operation module. The initial input current was set to 0.15 A and then changed with a 0.15 A-increment over a range of 1.35 A. Readings of the generated torques were recorded at each current increment. Also, generated torques were measured when the input current was set to 1.35 A and then adjusted with a 0.15 A-decrement over a range of 1.35 A. The performance of the guidewire operation module was tested through the same procedures. In addition, to investigate all the frictions during force and torque generation [i.e., discussed in (12) and (28)], experiments were carried out to measure the resistive force and resistive torque without generating force and torque feedback. In the resistive force measurements, to eliminate the interference of the motor, the coupling connecting the timing pulley to the motor was removed. Operations were performed with a linear speed of 0 mm/s with 1.5 mm/s-increments over a 12 mm/s range and a rotational speed of 0°/s with 40°/s-increments over a 360°/s range, respectively, [4], [27]. Also, at the same operating speed, the operations were performed with forward and reverse motions, and every operation was repeated nine times.

**2) Results and Discussion:** Similar to the discussion in Section V-A2, we only showed the experimental results of the catheter operation module rather than both the catheter operation module and guidewire operation module since they have similar performance. Experimental results of the catheter operation module are shown in Fig. 10. In the force generation experiments, the maximum error is 0.17 N, and the maximum relative error is 10.54%. The force generation error changes with the operation. Some tiny changes in the generated force would be lost when the expected force changes rapidly. Great errors generally occur in this case. For example, at approximately 3.4 s [see Fig. 10(a)], the force changes fast and the maximum error reaches 0.16 N. In gentle operations with a small force change rate, the error will be less than this value. Fig. 10(b) shows the results of the torque generation experiments. The maximum error is 1.17 mN•m and the maximum relative error is 12.36%. Great errors also occur when the expected torque changes rapidly. At about 8.6 s, the torque varies fast, and the maximum error reaches 0.88 mN•m.

The hysteretic characteristic of the catheter operation module is shown in Fig. 11. The measured torques form two curves with

different trends when the gradually increasing and decreasing currents are applied. It is mainly because of the hysteretic of the magnetic brake when various currents are used as the input. The maximum deviation between the torques with the increasing and decreasing currents is 0.85 mN•m. To reduce the influence of hysteresis on the torque feedback accuracy, we established a fitted curve based on these measured torques (dotted line in Fig. 11). The maximum deviation between the torque with the increasing current and the fitted torque is 0.54 mN•m; the maximum deviation between the torque with the decreasing current and the fitted torque is 0.53 mN•m. The relative errors for these two cases are 5.96% and 7.53%, respectively. The influence of hysteresis on torque feedback accuracy can be significantly reduced by using the fitted curve.

Fig. 12(a) and (b) show frictions during force and torque transmissions at various operating speeds. The average resistive forces for forward and reverse motions are 0.44 and 0.43 N, respectively; the average resistive torques for forward and reverse motions are 0.34 and 0.33 mN•m, respectively. Changes in motion speed seem to have little effect on friction. We think this is mainly because steel balls are placed between components that need to move relative to each other, e.g., slider and slider rail, and bearing, and almost all the frictions are rolling frictions. These measured values can be used for compensation during force and torque generation.

Fig. 12(c) displays the friction torque without the pantograph mechanism during torque transmission (i.e., initial resistive torque of the magnetic brake,  $T_{irt}$ ). The average values for forward and backward rotations are 1.97 and 1.92 mN•m, respectively, which are significantly larger than those when using the pantograph mechanism (i.e., 0.34 and 0.33 mN•m in Fig. 12(a) and (b)). This initial resistive torque cannot be eliminated, and its magnitude directly determines the accuracy of the torque feedback. When the pantograph mechanism is not employed, the minimum generated torque of the magnetic brake is 1.92 mN•m, since the initial resistive torque determines its minimum value. Even if a smaller torque can be generated using current control ( $T(i)$ ), positively correlated with the current  $i$ ), the final output of the magnetic brake is the sum of the initial resistive torque and the current-generated torque ( $T_{irt} + nT(i)_{min}$ , where  $n$  is the multiple controlled by the current and is a non-negative integer, and  $T(i)_{min}$  means the minimum torque generated by the minimum input current). When employing the pantograph mechanism,  $T_{irt} = 0.32$  mN•m,  $T(i)_{min} = 0.03$  mN•m, resulting in an output torque of  $0.32 + 0.03n$ ; conversely, without utilizing the pantograph mechanism,  $T_{irt} = 1.92$  mN•m,  $T(i)_{min} = 0.25$  mN•m, yielding an output torque of  $1.92 + 0.25n$ . Considering that  $n$  is a non-negative integer, the proposed method will achieve a high accuracy due to the significant reduction of  $T_{irt}$  and  $T(i)_{min}$ . Correspondingly, as illustrated in Fig. 11, it can be observed that when the input current is 0, the torque is 0.34 mN•m, which essentially represents  $T_{irt}$  after the implementation of the pantograph mechanism.

In addition, we obtained the output resolution of the haptic interface as 0.026 N for force generation and 0.03 mN•m for torque generation. We achieved this force resolution by compensating the friction force [see Fig. 12(a)] and

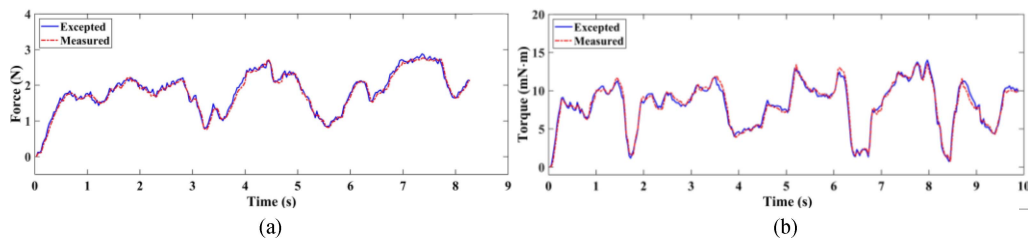


Fig. 10. Experimental results of the (a) force and (b) torque generation accuracy.

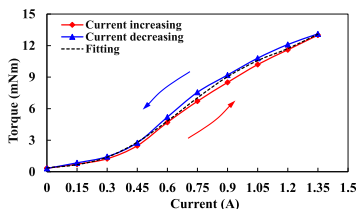


Fig. 11. Hysteretic characteristics of the catheter operation module.

implementing closed-loop control (14). Regarding torque resolution, we considered  $T(i)_{\min}$  as the resolution which is slightly different from the traditional one. Due to the initial resistance torque of catheters and guidewires in the blood vessels (caused by factors such as blood viscosity, frictional resistance, etc.), the actual torque during surgeries does not start from zero but is added on top of the initial resistance torque. The output torque of the proposed haptic interface is  $T_{irt} + nT(i)_{\min}$ , where  $T_{irt}$  and  $T(i)_{\min}$  have been significantly reduced by our proposed method. Although  $T_{irt}$  cannot be completely eliminated, it can be considered that it has been decreased below the initial resistance torque in the blood vessels. Besides, in [34], force resolution is defined as the smallest incremental force that can be generated in addition to the minimum force. Therefore, we consider it acceptable to use  $T(i)_{\min}$  as the torque resolution.

We also determined the response bandwidth of the proposed haptic interface, as illustrated in Fig. 13. Both force and torque responses exhibit a decrease in gain as the input frequency increases. The gain of force is  $-2.85$  dB at an input frequency of  $8.5$  Hz and declines to  $-4.15$  dB when the input frequency increases to  $9$  Hz. Similarly, at an input frequency of  $5.5$  Hz, the gain of torque is  $-2.97$  dB, which drops to  $-4.44$  dB when the input frequency rises to  $6$  Hz. Consequently, the bandwidths for force and torque are  $8.5$  and  $5.5$  Hz, respectively.

As shown in Fig. 11, the output torque reaches  $13.11$  mN·m when the input current is  $1.35$  A, and also, we obtained the maximum output force of the haptic interface is  $4.1$  N. Based on the analysis above, the proposed haptic interface satisfies sensing and feedback requirements (2) and (3) listed in Section II, and additionally, the proposed haptic interface would be helpful in retaining and utilizing interventionists' operating perception experience by providing reliable force and torque feedback.

### C. Workspace

1) *Experimental Set-Up*: In order to evaluate the attainable motions of the proposed haptic interface to satisfy the clinical

requirements for endovascular catheterization, the operating space for interventionists was investigated. Since interventionists hold the master catheter next to the catheter operation module to perform operations, we took the point on the master catheter at  $8$  mm away from the catheter operation module as the target point and calculated the movement space it can reach. Similarly, interventionists operate the torque device mounted on the end of the master guidewire, so the axis midpoint of the torque device was regarded as the target point. The distance of the torque device from the end of the master catheter was set as  $18$  mm according to the general operating habits of interventionists. The maximum bending angle of the mater catheter and guidewire was set as  $\pm 60^\circ$ . The workspace of these two target points was simulated through MATLAB based on the dimensional parameters of the haptic interface.

2) *Results and Discussion*: Fig. 14 shows the workspace of the proposed haptic interface. Colorful dots show the catheter operation workspace and gray points represent the guidewire operation workspace. The guidewire operation workspace is a cylinder with dimensions of  $\Phi 62.3$  mm  $\times$   $350$  mm, and the catheter operation workspace is an incomplete cylinder with dimensions of  $\Phi 27.7$  mm  $\times$   $350$  mm. In the workspace simulation, the maximum bending angle of the mater catheter and guidewire was set as  $\pm 60^\circ$ . The actual bending angle depends on the types of commercial catheters and guidewires. Since the proposed haptic interface uses commercial catheters and guidewires as the master catheters and guidewires and adopts the same operation paradigm as the actual surgical operation, the operating range in the  $x$ - and  $z$ -directions will meet the clinical requirements.

In the  $y$ -direction, the attainable operating distance is  $350$  mm, which is shorter than the actual operation requirement. To reduce the haptic interface dimension and decrease the influence on the accuracy of force/torque transmission caused by the long master guidewire, the operating range in the  $y$ -direction was designed with a smaller value. When the catheter/guidewire operation modules move to the extreme position [i.e., the catheter/guidewire operation modules are located at the right end of the slide rail in Fig. 3(a)], they need to be withdrawn to the initial position [i.e., the catheter/guidewire operation modules are placed to the left end of the slide rail in Fig. 3(a)]. The number of retracements depends on the type of catheters/guidewires operated by the slave manipulator (see Fig. 1). For example, the catheter operation module needs to be withdrawn one time when a catheter (451-550V0, Cordis, US) with a length of  $650$  mm is used for endovascular catheterization on the slave side. The maximum retracement number would be three since

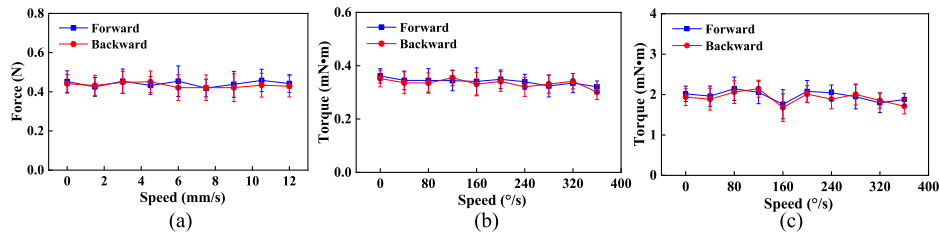


Fig. 12. Frictions during force and torque transmissions at various operating speeds: (a) resistive force; resistive torque (b) with and (c) without the pantograph mechanism.

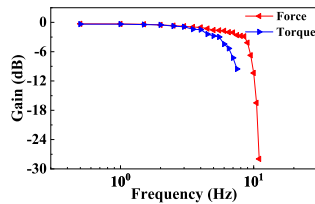


Fig. 13. Response bandwidth of the proposed haptic interface.

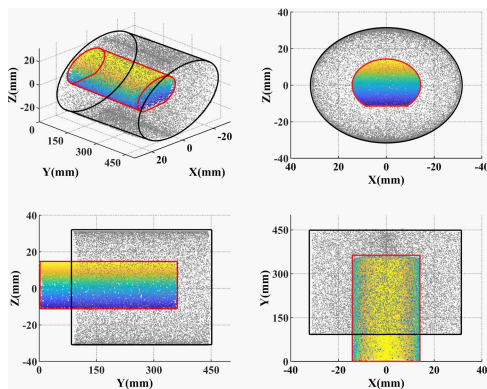


Fig. 14. Workspace of the proposed haptic interface.

the length of some special catheters/guidewires in endovascular catheterization can reach 1250 m, e.g., angiographic catheters (HNBR5.0-35-125-P-NS-DAV, COOK, US). Besides, the number of retracements of this proposed haptic interface is far less than that of almost all the commercial haptic devices or the existing research in [11], [12], [13], [14], [16], which have smaller workspaces than this proposed haptic interface. This design of the proposed haptic interface allows interventionists to operate with fewer retractions, offers an operating space similar to that in real procedures, and keeps a good balance between the device size and force/torque feedback accuracy. Therefore, the proposed haptic interface meets operating mode requirement (3) presented in Section II.

#### D. Operability

1) *Experimental Set-Up*: In the operability experiments, we investigated the operability of the proposed haptic interface by observing the operation performed by operators in the case of operating force and torque generation. The experimental data

obtained by our previous robots (presented in [4], [29]) as well as ATI force sensors in a human body model, were used to simulate the actual operating forces and torques. In the presence of the generated forces and torques, five interventionists with 1–8 years of clinical experience manipulated the master catheter and guidewire by push, pull, and rotation. The operating data was recorded by the proposed haptic interface. After the operation, interventionists were required to fill out questionnaires composed of the following eight questions:

- A-It is suitable for endovascular catheterization;
- B-It provides the same operating experience as the actual operation;
- C-It has the potential to increase the quality of robot-assisted endovascular catheterization;
- D-It is easy to control and the control unit is friendly;
- E-It provides both force and torque feedback that can be clearly perceived;
- F-It is easy to perform desired operations and the sense of touch to the operating handle is the same as the actual catheters and guidewires;
- G-It did not cause any discomfort during the operation;
- H-It deserves to be recommended to other users.

Ten points mean strong agreement, while zero point indicates strong disagreement.

2) *Results and Discussion*: Fig. 15 shows the displacement, force, rotation, and torque of the catheter and guidewire. The output forces are in the 0–3 N range and the output torques are in the 0–10 mN•m range. The collected motion is 0–350 mm and the captured rotation is in the range of  $-80^{\circ}$ – $240^{\circ}$ . The operator can use the proposed haptic interface to manipulate freely within its operating range. Due to the limitation of the workspace caused by the design parameters, the maximum operating displacement is 350 mm. However, there are no restrictions on the rotation operation and the operator can rotate the master catheter and guidewire at any angle.

The results of the questionnaires are shown in Fig. 16. The scores potentially indicate that operators may highly appreciate the operability of the proposed haptic interface. Especially, high scores on questions A, B, D, and F might prove that the proposed haptic interface meets operating mode requirements (1), (2), and (4) presented in Section II well from the perspective of users. Based on these observations, we think this proposed haptic interface would potentially be used in endovascular catheterization.

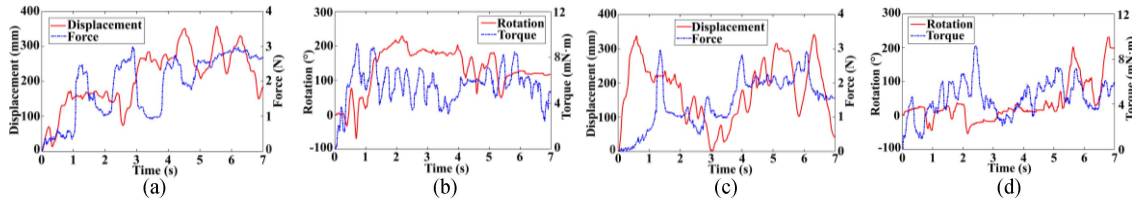


Fig. 15. Experimental results for the operability test. (a) Displacement and force of the catheter. (b) Rotation and torque of the catheter. (c) Displacement and force of the guidewire. (d) Rotation and torque of the guidewire.

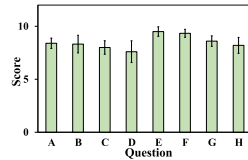


Fig. 16. Questionnaire scores for evaluating the operability.

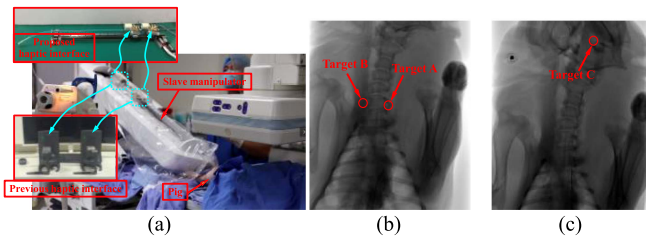


Fig. 17. (a) Animal experiment set-up, including two haptic interfaces, a slave manipulator, and a pig lying on the operating table. (b)–(c) Target points for animal experiments.

To further verify the feasibility, animal experiments were carried out in Section VI.

## VI. ANIMAL EXPERIMENTS

### A. Experimental Set-up

To test the possibility of clinical application of the proposed device and quantitatively evaluate its operating performance, comparative animal experiments were carried out. The experimental set-up is shown in Fig. 17(a). The slave manipulator proposed in our previous research [29] was set beside the operating table where a pig lay. The slave manipulator consists of a catheter manipulator and a guidewire manipulator and they are utilized to operate the commercial catheter and guidewire, respectively, on the slave side. Thus, as shown in Figs. 2 and 17(a), the catheter operation module of the proposed haptic interface (see Fig. 3) was used to control the catheter manipulator and the guidewire operation module was utilized to dominate the guidewire manipulator. To conduct comparative experiments, two commercial haptic devices (Geomagic TouchTMX, 3D Systems, Inc., USA) composed a haptic interface and worked as a “control group” since they can be regarded as a representative of current studies. The two commercial haptic devices dominated the catheter manipulator and guidewire manipulator, respectively [mapping relationship was shown in Fig. 17(a)]. These two types of haptic interfaces were located outside the operating room.

In these experiments, three tasks (tasks A, B, and C) were set and selected for tasks A, B, and C, respectively. In each task, the catheter needed to be propelled from the femoral artery to the target point. Fig. 17(b) and (c) shows the positions of the three targets. Targets A and B are in the left vertebral artery and right vertebral artery near the neck, respectively; target C is located in the left carotid artery in the brain. To quantitatively assess the characteristics of the proposed haptic interface, two metrics were selected to evaluate the performance of the haptic interface and the workload of interventionists. 1) Completion time: It is the total time used by the interventionist to propel the catheter and guidewire to the target point. Lower completion time is an indicator of better performance of the proposed haptic interface. 2) NASA-TLX: It is a task load index developed by NASA-Ames Research Center for workload assessment [32]. It consists of six dimensions of workload and the users complete the questionnaire with various scores ranging from 0 to 100. A higher NASA-TLX score represents a heavier workload.

Five interventionists, all males aged 27 to 56 years (average 41.2, SD 11.7), were involved in the animal experiments. They have 2 to 32 years of clinical experience (average 16.4, SD 12.6). These participants were told about the characteristics and operation method of the device before each trial. The procedure is composed of the following three steps:

- 1) the participant uses the device (i.e., proposed haptic interface and previous interface) to complete the tasks (tasks A, B, and C) by propelling the catheter to the target points (targets A, B, and C);
- 2) the completion time is recorded and the participant fills out the NASA-TLX questionnaires;
- 3) the participant repeats the trial three additional times for each task. Analysis of variance (ANOVA) was conducted on all the metrics, and post-hoc pairwise comparisons would be used for further analysis by using the least significant difference (LSD) when necessary.

The results were considered significant when the alpha was below 0.05.

### B. Results and Discussion

One trial was not completed since the pig woke up during this trial. These experiments lasted too long and the anesthetic lost efficacy before the end of the experiments. If a participant failed to propel the catheter to the target, he would try to withdraw the catheter and guidewire a bit and continue the operation until it

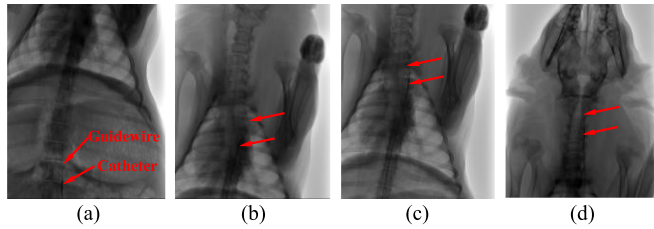


**Fig. 18.** Operation process of task C. (a) Catheter and guidewire were advancing from the femoral artery to the aortic arch. (b) Catheter and guidewire entered the aortic arch. (c) Catheter and guidewire started looking for the entrance to the left carotid artery. (d) Catheter and guidewire entered the left carotid artery and tried to move to the target point.

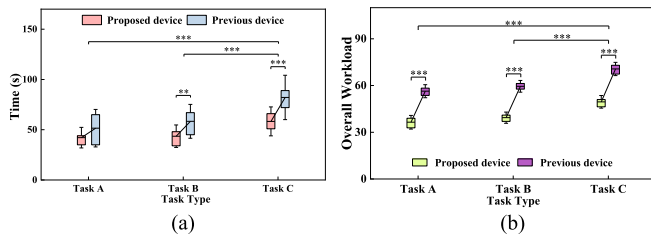


**Fig. 19.** Statistical analysis on the completion time (a) and overall workload comparison (b). Three horizontal lines of the box represent the first custom quartile (30th), the sample median, and the third custom quartile (70th). Error bars indicate the standard deviation. \*, \*\*, and \*\*\* represent the significant level of 0.05, 0.01, and 0.001, respectively.

succeeded. Thus, the completion time increased and this case would not be counted as a failed trial.

Since task C was much more complex, we chose the operation process of task C as the demonstration. As shown in Fig. 18, with the cooperation of catheters and guidewires, the catheter and guidewire started to advance from the femoral artery and then passed through the aortic arch. After entering the left carotid artery, they finally reached target C.

Fig. 19(a) shows the effort of the task type and device type on the completion time for the experiments. The effort of the task type on the completion time was significant,  $F(2, 116) = 30.10, p < 0.001$ . Post-hoc pairwise comparisons showed that the difference between tasks B and C, and the difference between tasks A and C, was significant with  $p < 0.001$ . In task A, the interventionist completed the task faster when using the proposed haptic interface (average 42.15 s, SD 9.98 s) and slower when using the previous haptic interface (average 51.55 s, SD 18.15 s). Similar situations occurred in tasks B and C. This may be explained by that the proposed haptic interface retains the tactile sensation, exploits prior dexterous skills of interventionists, and also allows interventionists to operate with fewer retractions of the master catheter/guidewire (fewer retractions were discussed in Section V-C2). Moreover, the effort of the device type on the completion time of all tasks was significant,  $F(1, 117) = 15.14, p < 0.001$ . For tasks B and C, the effort of the device type on the completion time was all significant ( $F(1,37) = 10.72, p < 0.01; F(1,37) = 16.42, p < 0.001$ ). However, surprisingly, for task A, there was no significant effort of the device type on

the completion time ( $F(1, 37) = 1.83, p = 1.18$ ). We think task A was not that complex and the advantage of the proposed haptic device had not been revealed. These results demonstrated that both the device type and task type seemed to affect the completion time, and the proposed haptic interface appeared to have better performance than the previous haptic interface.

The overall workload comparison is shown in Fig. 19(b). The effort of the task type on the overall workload was significant,  $F(2, 116) = 23.19, p < 0.001$ . Post-hoc pairwise comparisons showed that the difference between each task for the overall workload was coherent with that for the completion time. Namely, the difference between tasks B and C, and the difference between tasks A and C, was significant with  $p < 0.001$ . Besides, tasks A and B had a similar overall workload value, while the overall workload of task A (average 46.42, SD 10.81) was less than that of task C (average 60.31, SD 11.51). Thus, different tasks seemed to result in various overall workloads and the complex task appears to require a heavy workload. The effort of the device type on the overall workload of all tasks was significant,  $F(1, 117) = 83.13, p < 0.001$ . For tasks A, B, and C, the effort of the device type on the overall workload was all significant with  $p < 0.001$ . The overall workload of the proposed haptic interface was less than that of the previous haptic interface in all tasks. For example, in task C, the overall workload of the proposed haptic interface is  $49.53 \pm 3.95$ , while the overall workload of the previous haptic interface is  $71.09 \pm 4.09$ . Thus, the proposed haptic interface appeared to be easier to use.

Fig. 20 shows the statistical analysis on the six dimensions of the workload. The task type had significant effects on the five workload dimensions: Mental Demand ( $F(2, 116) = 16.52, p < 0.001$ ), Physical Demand ( $F(2, 116) = 24.50, p < 0.001$ ), Temporal Demand ( $F(2, 116) = 17.59, p < 0.001$ ), Performance ( $F(2, 116) = 28.71, p < 0.001$ ), and Effort ( $F(2, 116) = 13.19, p < 0.001$ ). In these five dimensions, post-hoc pairwise comparisons showed that the difference between tasks B and C, and the difference between tasks A and C, was significant with  $p < 0.001$ . This situation was also seen in the completion time and the overall workload. We think this is mainly because tasks A and B have similar catheter/guidewire propelling displacement and similar operation difficulty. The device type had significant effects on all the six workload dimensions: Mental Demand ( $F(1, 117) = 49.10, p < 0.001$ ), Physical Demand ( $F(1, 117) = 10.71, p < 0.05$ ), Temporal Demand ( $F(1, 117) = 32.62, p < 0.001$ ), Performance ( $F(1, 117) = 26.89, p < 0.001$ ), Effort ( $F(1, 117) = 37.57, p < 0.001$ ), and Frustration ( $F(1, 117) = 89.36, p < 0.001$ ). In each task, the effect of the device type on all the workload dimensions was significant with  $p < 0.001$ , except for a significant effect on Physical Demand with  $p < 0.05$ . In particular, in the Frustration test, the score for the proposed haptic interface (average 33.80, SD 6.99) was far less than that for the previous haptic interface (average 87.23, SD 5.80). The proposed haptic interface adopting real commercial catheters and guidewires and retaining the actual operating mode, can enable interventionists to utilize their accumulated clinical operating experience entirely, resulting in lower scores in the Frustration test.

Based on the experimental results, we found that the proposed haptic interface can control the slave manipulator and

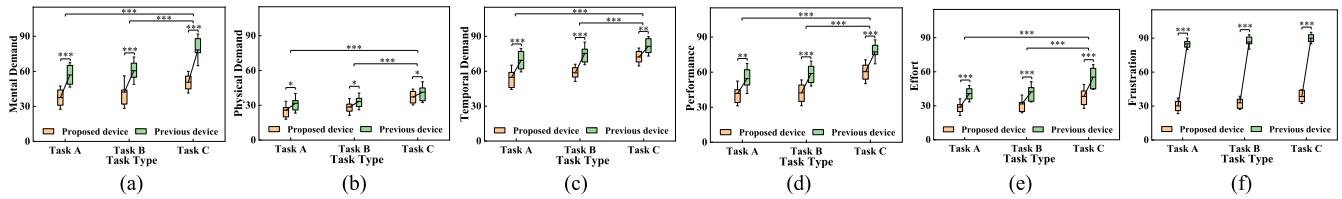


**Fig. 20.** Six dimensions of the workload. (a) Mental demand. (b) Physical demand. (c) Temporal demand. (d) Performance. (e) Effort. (f) Frustration. Three horizontal lines of the box represent the first custom quartile (30th), the sample median, and the third custom quartile (70th). Errors bars indicate the standard deviation. \*, \*\*, and \*\*\* represent the significant level of 0.05, 0.01, and 0.001, respectively.

complete various operations successfully, and thus this proposed device potentially has good feasibility for clinical application. In addition, all results of the comparison experiments show that the proposed haptic interface consumes less operation time and requires a lighter workload (especially for the frustration test) than the commercial haptic devices, which means that the proposed haptic interface appears to have good operating performance. The performance associated with the proposed haptic interface and commercial haptic devices may not characterize their usability strictly, but they can be regarded as a good first approximation and base of comparison.

## VII. CONCLUSION

In this article, we developed a novel haptic interface that can retain interventionists' prior clinical operating experience, including motion perception, force feedback, torque feedback, tactile sensation, and operating mode. The performance was evaluated through simulations, laboratory experiments, and animal experiments. Experimental results show that the proposed haptic interface appears to have good performance and potential further applications in robot-assisted endovascular catheterization. The haptic interface satisfies all the design requirements proposed in Section II, and it would have the following advantages when integrated into the robot-assisted endovascular catheterization:

- 1) The system operability and operation safety will be enhanced potentially since more comprehensive operating information is transmitted to the operator by producing force and torque of both catheters and guidewires.
- 2) By retaining the tactile sensation and traditional operating mode, the proposed haptic interface will enable interventionists to utilize their prior accumulated clinical operating experience.
- 3) Since interventionists can manipulate the proposed haptic interface in the traditional way they are used to, the operation will be performed with a light workload and much pleasure.

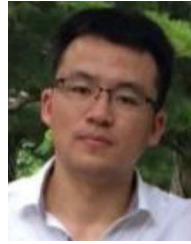
In addition, this proposed haptic interface has potential applications in integration with virtual reality training systems to train inexperienced interventionists. However, some limitations still exist in this research. The transmission components of the proposed haptic interface are bare, such as the timing belts, couplings, and gears. These components need to be packaged properly to make the proposed haptic interface look more friendly. In animal experiments, the number of tasks, participants, and trials

is not enough to comprehensively evaluate the performance. More animal experiments and in-human experiments need to be conducted in future research.

## REFERENCES

- [1] H. Rafii-Tari et al., "Current and emerging robot-assisted endovascular catheterization technologies: A review," *Ann. Biomed. Eng.*, vol. 42, no. 4, pp. 697–715, 2014.
- [2] S. Au et al., "Robotic endovascular surgery," *Asian Cardiovasc. Thoracic Ann.*, vol. 22, no. 1, pp. 110–114, Jan. 2014.
- [3] A. Hooshiar, S. Najarian, and J. Dargahi, "Haptic telerobotic cardiovascular intervention: A review of approaches, methods, and future perspectives," *IEEE Rev. Biomed. Eng.*, vol. 13, pp. 32–50, Apr. 2020.
- [4] X. Bao et al., "A cooperation of catheters and guidewires-based novel remote-controlled vascular interventional robot," *Biomed. Microdevices*, vol. 20, no. 1, pp. 20–38, 2018.
- [5] N. Lo et al., "Robotic-assisted percutaneous coronary intervention," *Curr. Treat. Options Cardiovasc. Med.*, vol. 20, no. 2, pp. 14–23, Feb. 2018.
- [6] K. Wang et al., "Endovascular intervention robot with multi-manipulators for surgical procedures: Dexterity, adaptability, and practicability," *Robot. Comput.-Integr. Manuf.*, vol. 56, pp. 75–84, 2019.
- [7] A. Hooshiar, A. Sayadi, J. Dargahi, and S. Najarian, "Integral-free spatial orientation estimation method and wearable rotation measurement device for robot-assisted catheter intervention," *IEEE/ASME Trans. Mechatron.*, vol. 27, no. 2, pp. 766–776, Apr. 2022.
- [8] M. Tavallaei et al., "Design, development and evaluation of a compact telerobotic catheter navigation system," *Int. J. Med. Robot. Comput. Assist. Surg.*, vol. 12, no. 3, pp. 442–452, 2016.
- [9] Y. Thakur, J. S. Bax, D. W. Holdsworth, and M. Drangova, "Design and performance evaluation of a remote catheter navigation system," *IEEE Trans. Biomed. Eng.*, vol. 56, no. 7, pp. 1901–1908, Jul. 2009.
- [10] N. K. Sankaran, P. Chembrammal, A. Siddiqui, K. Snyder, and T. Kesavadas, "Design and development of surgeon augmented endovascular robotic system," *IEEE Trans. Biomed. Eng.*, vol. 65, no. 11, pp. 2483–2493, Nov. 2018.
- [11] C. Meng et al., "A remote-controlled vascular interventional robot: System structure and image guidance," *Int. J. Med. Robot. Comput. Assist. Surg.*, vol. 9, no. 2, pp. 230–239, 2013.
- [12] H. Shen et al., "A novel robotic system for vascular intervention: Principles, performances, and applications," *Int. J. Comput. Assist. Radiol. Surg.*, vol. 14, pp. 671–683, 2019.
- [13] H. -J. Cha, H. -S. Yoon, K. Y. Jung, B. -J. Yi, S. Lee, and J. Y. Won, "A robotic system for percutaneous coronary intervention equipped with a steerable catheter and force feedback function," in *Proc. IEEE/RSJ Int. Conf. Intell. Robots Syst.*, Oct. 2016, pp. 1151–1156.
- [14] H. Cha et al., "An assembly-type master-slave catheter and guidewire driving system for vascular intervention," *Proc. Inst. Mech. Eng., Part H, J. Eng. Med.*, vol. 231, no. 1, pp. 69–79, 2017.
- [15] J. Woo et al., "Advantage of steerable catheter and haptic feedback for a 5-DOF vascular intervention robot system," *Appl. Sci. (Basel)*, vol. 9, pp. 4035–4048, 2019.
- [16] Z. Feng et al., "Design and evaluation of a bio-inspired robotic hand for percutaneous coronary intervention," in *Proc. IEEE Int. Conf. Robot. Automat.*, 2015, pp. 5338–5343.
- [17] H. Wang et al., "Research on a novel vascular interventional surgery robot and control method based on precise delivery," *IEEE Access*, vol. 9, pp. 26568–26582, 2021.

- [18] X. Yin, S. Guo, N. Xiao, T. Tamiya, H. Hirata, and H. Ishihara, "Safety operation consciousness realization of a MR fluids-based novel haptic interface for teleoperated catheter minimally invasive neuro surgery," *IEEE/ASME Trans. Mechatron.*, vol. 21, no. 2, pp. 1043–1054, Apr. 2016.
- [19] S. Guo et al., "A novel robot-assisted endovascular catheterization system with haptic force feedback," *IEEE Trans. Robot.*, vol. 35, no. 3, pp. 685–696, Jun. 2019.
- [20] J. C. Payne, H. Rafii-Tari, and G.-Z. Yang, "A force feedback system for endovascular catheterisation," in *Proc. IEEE/RSJ Int. Conf. Intell. Robots Syst.*, Vilamoura-Algarve, Portugal, Oct. 2012, pp. 1298–1304.
- [21] J. W. Park et al., "Development of a force-reflecting robotic platform for cardiac catheter navigation," *Artif. Organs*, vol. 34, no. 11, pp. 1034–1039, Nov. 2010.
- [22] L. Cerenelli et al., "CathROB: A highly compact and versatile remote catheter navigation system," *Appl. Bionics Biomech.*, vol. 2017, May 2017, Art. no. 2712453.
- [23] M. Abdelaziz et al., "Toward a versatile robotic platform for fluoroscopy and MRI-Guided endovascular interventions: A pre-clinical study," in *Proc. IEEE/RSJ Int. Conf. Intell. Robots Syst.*, Nov. 2019, pp. 5411–5418.
- [24] N. Xiao et al., "Internet-based robotic catheter surgery system-system design and performance evaluation," in *Proc. IEEE Int. Conf. Automat. Logistics*, Aug. 2012, pp. 645–651.
- [25] L. Jones, "Kinesthetic sensing," in *Human and Machine Haptics*, M. Cutkosky, Ed., Cambridge, MA, USA: MIT Press, 2000.
- [26] L. Jandura et al., "Experiments on human performance in torque discrimination and control," in *Time-Varying Systems and Control*, vol. 1, C. J. Radcliffe, Ed., New York, NY, USA: ASME, 1994, pp. 369–375.
- [27] H. Rafii-Tari et al., "Assessment of navigation cues with proximal force sensing during endovascular catheterization," *Med. Image. Comput. Comput. Assist. Interv.*, vol. 15, pp. 560–567, Sep. 2012.
- [28] X. Bao et al., "Multilevel operation strategy of a vascular interventional robot system for surgical safety in teleoperation," *IEEE Trans. Robot.*, vol. 38, no. 4, pp. 2238–2250, Aug. 2022.
- [29] X. Bao et al., "Operation evaluation in-human of a novel Remote-controlled vascular interventional robot," *Biomed. Microdevices*, vol. 20, no. 2, pp. 34–47, Apr. 2018.
- [30] T. Endo et al., "Five-fingered haptic interface robot: HIRO III," *IEEE Trans. Haptics*, vol. 4, no. 1, pp. 14–27, Jan.–Mar. 2011.
- [31] D. Wang et al., "Toward whole-hand kinesthetic feedback: A survey of force feedback gloves," *IEEE Trans. Haptics*, vol. 12, no. 2, pp. 189–204, Apr. 2019.
- [32] S. Hart et al., "Development of NASA-TLX (Task load index): Results of empirical and theoretical research," in *Human Mental Workload*, vol. 52, P. Hancock et al., Ed., New York, NY, USA: Elsevier, 1988, pp. 139–183.
- [33] T. L. Brooks, "Telerobotic response requirements," in *Proc. IEEE Int. Conf. Syst., Man, Cybern.*, 1990, pp. 113–120.
- [34] E. Samur, "Performance evaluation based on psychophysical tests," in *Performance Metrics for Haptic Interfaces*. London, U.K.: Springer-Verlag, 2012, pp. 81–106.



**Xianqiang Bao** (Member, IEEE) received the Ph.D. degree in biomedical engineering from Beijing Institute of Technology, Beijing, China, in 2019.

He held a position as a Research Fellow in the Department of Biomedical Engineering, King's College London, London, U.K. Since 2022, he has been engaged with the Physical Intelligence Department, Max Planck Institute for Intelligent Systems, Stuttgart, Germany, serving as a Humboldt Fellow under the patronage of the Alexander von Humboldt Foundation. His research interests include medical robotics, magnetically controlled microrobots, soft robotics, robotic ultrasound, force control, and haptic feedback.



**Shuxiang Guo** (Fellow, IEEE) received the Ph.D. degree in mechanoinformatics and systems from Nagoya University, Nagoya, Japan, in 1995.

He is currently a Chair Professor with the Department of Electronic and Electrical Engineering, Southern University of Science and Technology, Shenzhen, China, and also a Chair Professor with the Key Laboratory of Convergence Medical Engineering System and Healthcare Technology, Ministry of Industry and Information Technology, Beijing Institute of Technology, Beijing, China. His research interests include medical robot systems, microcatheter systems, and biomimetic underwater robots.

Dr. Guo is the Fellow of The Engineering Academy of Japan.



**Cheng Yang** received the M.Eng. degree in control engineering from the Beijing Institute of Technology, Beijing, China, in 2018, where he is currently working toward the Ph.D. degree.

His research interests include medical robotics.



**Lingling Zheng** received the Ph.D. degree in intelligent mechanical systems engineering from the Faculty of Engineering and Design, Kagawa University, Kagawa, Japan, in 2022.

She is currently an Assistant Professor with the School of Information Engineering and the School of Artificial Intelligence, Nanjing Xiaozhuang University, Nanjing, China. Her current research interests include medical robots and microrobots.